4th URSI AT-RASC, Gran Canaria, 19 – 24 May 2024

Polarization Characterization of THz Scattering from Rough Surfaces based on Deep Learning

Xu Zhao(1), Ben Chen(2), Ke Guan(3)(2), Bin Lu(1), Yao Wei(1), and Mingyang Dong(1)
(1) Research Institute of China Telecom Co., Ltd., 109 West Zhongshan Ave., Tianhe District, Guangzhou 510630, China
(2) School of Electronic and Information Engineering, Beijing Jiaotong University, Beijing 100044, China
(3) State Key Laboratory of Advanced Rail Autonomous Operation, Beijing Jiaotong University, Beijing 100044, China

Abstract

With the increasing demand for data transmission, researchers are getting interested in the topic of terahertz (THz) communication systems. As an important parameter of electromagnetic wave propagation, polarization is critical for THz channel modeling. In the previous work, a deep learning (DL)-based THz scattering model has been proposed to reconstruct the scattered electric field on the rough Perfect electric conductor (PEC) surface in the far-field region of the upper hemisphere space. For further refinement, the model is retrained in this paper, and the polarization characteristics of the scattered electric field for both Transverse Magnetic (TM)- and Transverse Electric (TE)-polarized incidence are analyzed in terms of the cross-polarization power ratio (XPR) and the Poincaré sphere. Finally, a scattering model covering multiple dimensions such as amplitude and polarization is expected to be realized.

1 Introduction

To provide transmission services with higher data rates and lower time delays, THz communications and relevant technologies are gradually becoming a hot research spot [1][2]. While designing THz communication systems, polarization characteristics play a significant role in both signal transmission and system performance. In addition, when interacting with dielectric materials, THz waves with different polarizations exhibit distinctive reflection, scattering, and transmission characteristics [3]. However, due to the short wavelength, the scattering behavior of THz waves is particularly affected by the surface roughness, leading to scattering with complex polarization characteristics.

Currently, despite the hardware limitation, some measurements and modeling works have been presented for THz wave polarization. The authors of [4] conducted measurement campaigns at the 300 GHz band for scenarios of "smart rail mobility" and concluded that the XPR decreases rapidly in the absence of line-of-sight (LOS) paths, leading to severe depolarization. A 190 GHz indoor measurement was presented in work [5], finding that the XPR of the non-LOS (NLOS) path is not only affected by the polarization modes of the transceivers but also related to the structure of the reflection surfaces. In work [3], the scattering of incident waves with different polarizations at the 300 GHz band was meticulously analyzed based on the theory of the stochastic functional approach. Meanwhile, the authors of [6] introduced an improved Finite-Difference Time-Domain (FDTD) method for rough surface scattering and analyzed the modeling results with TE- and TM-polarized incidence.

Due to the effect of randomness, the accuracy of rough surface scattering reconstructed by the statistic model is relatively low, while traditional electromagnetic computational methods are challenged with high computational demands and extended processing times in the THz band. Therefore, to balance accuracy and efficiency, in previous studies, we have proposed a DL-based surface current generation model and demonstrated its ability to accurately reconstruct the scattered electric field (mainly the amplitude) in the far field when the incident wave is TM-polarized [7]. In this paper, the database of TE-polarized incidence is extended to explore the adaptability of the model to different polarized incidence waves, and the DL-based model is retrained based on it. Furthermore, two effective polarization analysis methods are used to validate the accuracy of the polarisation characteristics of the reconstructed scattered electric field. Firstly, the XPR distribution of the scattering points statistically analyzed to offer a initial assessment of the reconstructed polarization. Subsequently, the Poincaré sphere is employed to illustrate the polarization at each scattering point for further examining the accuracy of the reconstructed polarization characteristics. The rest of the paper is organized as follows: Section II briefly describes the structure of the DL-based model and the database constructed by full-wave simulations. Section III analyses the polarization characteristics of the scattered electric field with the XPR distribution and Poincaré sphere. Finally, the conclusion is given in Section IV.

2 Research methodology

2.1 Database and DL-based Model

Using the full-wave simulation software Feko, we design 300 GHz simulation scenarios with multiple incidence directions and multiple rough surfaces, and the specific simulation parameters are detailed in Table 1.

Table 1. Simulation configuration of the database

Incident wave	Amplitude	1 V/m
	Polarization	TM/TE
	Frequency	300 GHz
	Incidence angle θ [°]	0, 10, 20, 30, 40, 50, 60, 70, 80
	Azimuth angle φ [°]	0, 5, 10, 15, 20, 25, 30, 35, 40, 45
Rough surface	Area	35 mm × 35 mm
	Material	Perfect electric conductor
	Correlation length l [mm]	1.0, 1.5, 2.0, 2.5, 3.0
	Root-Mean-Square height δ [mm]	0.05, 0.10, 0.15, 0.20, 0.25

According to the different polarization modes of the incident waves, we obtained the TM and TE polarization databases and trained the DL-based model respectively (the TM polarization database has been trained in the previous work). The architecture of the model is presented in Fig. 1, which includes four parts: the input, processing module, generation module, and output. The processing module contains a surface processing branch (consisting of residual blocks) and two angle processing branches (consisting of fully connected layers). The generation module contains three generation branches (consisting of multilayer modulated convolutional and residual layers) of the x, y, and z components of the surface currents - J_x, J_y, and J_z. The final outputs of the model are Real and imaginary parts of J_x, J_y, and J_z , which will be further used to calculate the scattered electric field, based on the Dyadic Green's function theorem [8].

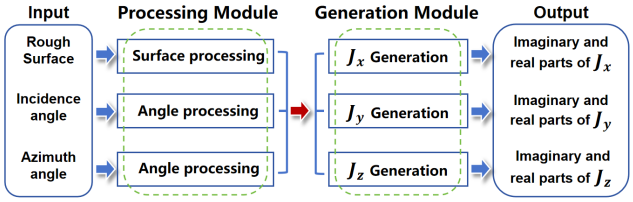

Figure 1. The architecture of the DL-based surface current generation model [7]

2.2 Analysis methods for polarization

The XPR is used to evaluate the depolarization of the channel, which is defined as the ratio for the component of the received electric field that is co-polarized with the transmitted field, to the component that is cross-polarized. As shown in Fig. 2, $\vec{E}_{i,TE}$ and $\vec{E}_{i,TM}$ are the electric field vectors of the incident wave for TE and TM polarization, respectively. $\vec{E}_\theta$ and $\vec{E}_\varphi$ are the components of the scattered electric field at θ and φ directions in the spherical coordinate system, respectively. Therefore, when the incident wave is TE-polarized, the co-polarized component of the scattered electric field is $\vec{E}_\varphi$ and the cross-polarized component is $\vec{E}_\theta$.The opposite conclusion is reached when the incident wave is TM-polarized. The XPR is expressed as:

$$XPR = \begin{cases} 20\log_{10}(|\vec{E}_\theta|/|\vec{E}_\varphi|), & \text{TM-polarized incidence} \\ 20\log_{10}(|\vec{E}_\varphi|/|\vec{E}_\theta|), & \text{TE-polarized incidence} \end{cases}. \quad (1)$$

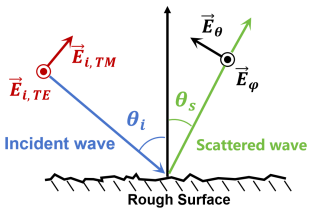

Figure 2. Polarization of incident and scattered electric fields

Although the incident electric field is linear polarization, the polarization mode of the scattered electric field is significantly affected by the rough surface and thus behaves more as an elliptical polarization, i.e. the end of the electric field vector forms an elliptic trace in space as shown in Fig. 3 (a), where ψ is the tilt angle and χ is the ellipticity angle, defined as follows [9][10]:

$$\psi = \frac{1}{2}\tan^{-1}\left(\frac{S_2}{S_1}\right), \chi = \frac{1}{2}\sin^{-1}\left(\frac{S_3}{S_0}\right) \quad (2)$$

where S_0, S_1, S_2, S_3 are Stokes polarization parameters:

$$S_0 = |\vec{E}_\theta|^2 + |\vec{E}_\varphi|^2 \quad (3a)$$
$$S_1 = |\vec{E}_\theta|^2 - |\vec{E}_\varphi|^2 \quad (3b)$$
$$S_2 = 2|\vec{E}_\theta||\vec{E}_\varphi|\cos\delta \quad (3c)$$
$$S_3 = 2|\vec{E}_\theta||\vec{E}_\varphi|\sin\delta \quad (3d)$$

where δ denotes the difference between the phases of $\vec{E}_\varphi$ and $\vec{E}_\theta$. The normalized Stokes parameters s_1, s_2 and s_3 are obtained by normalizing S_1, S_2 and S_3 (divide by $\sqrt{S_1^2+S_2^2+S_3^2}$). The polarization point with coordinates (s_1,s_2,s_3) can be represented on a sphere with radius 1, which is known as the Poincaré sphere, as shown in Fig. 3 (b). Derived from Eq. (2), 2ψ and 2χ are the azimuth and elevation angles of the Poincaré sphere, respectively.

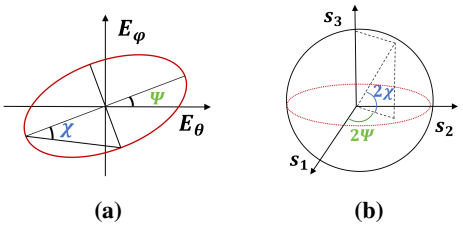

Figure 3. (a) Polarization ellipse and (b) Poincaré sphere

The Poincaré sphere can visually represent all the polarization modes of the electric field, including line polarization, circular polarization and elliptical polarization. For example, TM polarization point is represented as (1, 0, 0) while TE polarization point as (-1, 0, 0) .

3 Polarization Analysis

Based on the test set, in this section, we validate the model's ability to reconstruct the scattering polarization in various conditions.

3.1 Different Rough Surfaces

With the decrease of l and the increase of δ, the surface roughness is subsequently elevated, and the distribution of the scattered energy in the upper hemispherical surface becomes more dispersed. We select the energy-concentrated regions around the specular reflection direction (90% of the total energy) and statistically analyze the XPR within the region, as shown in Fig. 4. As can be seen, the reconstructed XPR histograms agrees perfectly with the simulation results. Logistic distribution has a better fit to the peaks and tails of the data distribution and is utilized to fit the XPR in this paper, XPR$\sim$*Logistic*(μ_L, σ_L), where μ_L is the position parameter and σ_L is the scale parameter. The fitting parameters for the XPR of different rough surfaces are listed in Table 2. When the roughness is the smallest (l=0.3 mm, δ=0.05 mm), the μ_L reaches the maximum of 20.29 dB at TM-polarized incidence and 20.15 dB at TE-polarized incidence. With the increasing roughness, the μ_L becomes smaller subsequently, which indicates that the large roughness causes significant depolarization in the THz transmission. In addition, the errors of each fitting parameter of the model are less than 2.5 dB, proving that the model can well predict the polarization characteristics, both TE-and TM- polarized incidence.

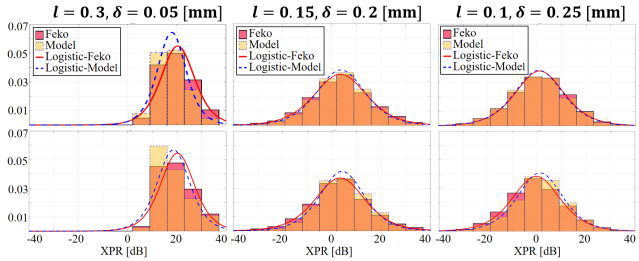

Figure 4. XPR of the scattered electric field for different rough surfaces (the first line is for TM-polarized incidence and the second line is for TE-polarized incidence)

Table 2. Fitting parameters for XPR

	Roughness [mm]	Feko [dB]		Model [dB]		Error [dB]	
		μ_L	σ_L	μ_L	σ_L	μ_L	σ_L
TM	l=0.3, δ=0.05	20.29	4.55	17.86	3.88	2.43	0.67
	l=0.15, δ=0.2	3.55	7.10	3.73	6.54	-0.18	0.56
	l=0.1, δ=0.25	1.08	6.63	0.69	6.54	0.39	0.09
TE	l=0.3, δ=0.05	20.15	4.58	18.58	4.39	1.57	0.19
	l=0.15, δ=0.2	3.24	6.72	4.07	5.97	-0.83	0.75
	l=0.1, δ=0.25	-0.35	6.49	1.22	6.11	-1.57	0.38

Fig. 5 illustrates the distribution of the polarization points of the scattered electric field in the energy-concentrated region on the Poincaré sphere for different roughness conditions at TM- and TE-polarized incidence. When the roughness is smallest, the polarization points are mainly distributed around the s_1 axis of the Poincaré sphere, suggesting a less severe depolarisation at this moment. For both TE- and TM-polarized incidence, as the roughness increases, the polarization points begin to align more along the equatorial plane (the s_1s_2 plane) of the Poincaré sphere, implying the appearance of different morphological line polarization modes. Concurrently, there is a noticeable diffusion of polarization points towards the poles of the Poincaré sphere, indicative of an increasing prominence of elliptical polarization. These trends are well characterized by the reconstructed polarization points of the model, which are in high agreement with the simulation results.

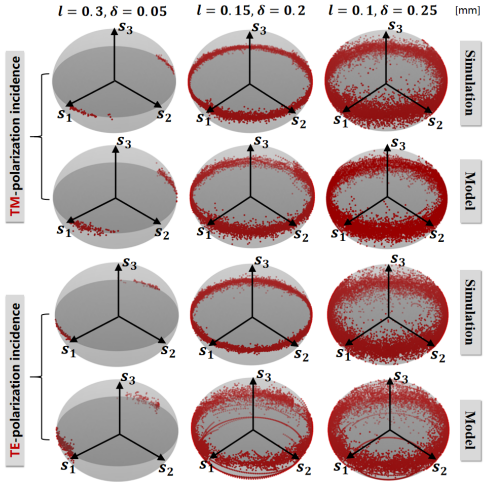

Figure 5. Distribution of polarization points on the Poincaré sphere for different rough surfaces

3.2 Different Incidence Angles

Fig. 6 illustrates the distribution of XPR for different incidence angles, and the logistic fitting parameters are listed in Table 3. A tendency for the μ_L of the XPR to become larger with increasing incidence angle can be observed for both TE- and TM-polarized incidence, implying that the depolarization is weaker for large incidence angles. Meanwhile the errors of each fitting parameter of the model are less than 1 dB except for the case of θ=50°, implicating the accuracy of the model in predicting the XPR for small incidence angles. The distributions of scattering polarization points on the Poincaré sphere for different incidence angles with TE- and TM-polarized incidence are shown in Fig. 7. As the incidence angle increases, the polarization

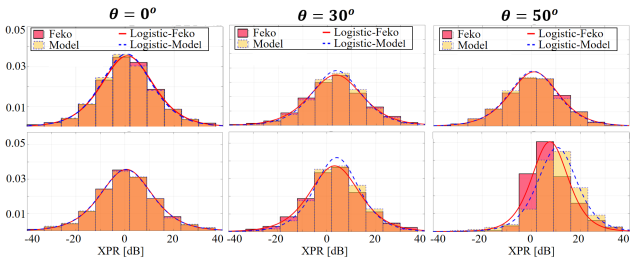

Figure 6. XPR of the scattered electric field for different incidence angles (the first line is for TM-polarized incidence and the second line is for TE-polarized incidence)

Table 3. Fitting parameters for XPR

	Incidence angle[°]	Feko [dB]		Model [dB]		Error [dB]	
		μ_L	σ_L	μ_L	σ_L	μ_L	σ_L
TM	0	0.94	7.05	0.59	6.86	0.35	0.19
	30	3.55	7.10	3.73	6.54	-0.18	0.56
	50	8.42	5.26	6.57	5.74	1.85	-0.48
TE	0	0.62	7.00	0.50	7.03	0.12	-0.03
	30	3.24	6.72	4.07	5.97	-0.83	0.75
	50	7.51	4.95	10.54	5.29	-3.03	-0.34

points gradually spread around from the equatorial plane. The model is in good agreement with the simulation results, demonstrating robust prediction ability for scattering polarization at different incidence angles.

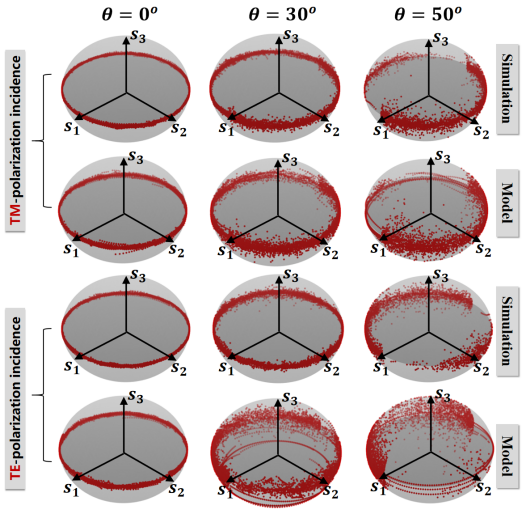

Figure 7. Distribution of polarization points on the Poincaré sphere for different incidence angles

4 Conclusion

In this study, to validate the ability of the surface current generation model to reconstruct the polarization of the scattered electric field, we analyze the XPR distribution and visualize the polarization using the Poincaré sphere. The results show that the model can accurately reconstruct the polarization characteristics of the scattered electric field, especially for different incidence angles and different rough surfaces. Specifically, the error in the fitting parameters of the logistic distribution of the XPR is within 1 dB when the incidence angle is less than 50°. In addition, the distributions of the reconstructed polarization points on the Poincaré sphere are in basic agreement with the simulation results. These studies provide a solid foundation for us to extend the application of the model to scattering from dielectric material in the future.

5 Acknowledgements

This work was supported by the National Key Research and Development Program of China under Grant 2021YFB2900300.

References

[1] I. F. Akyildiz, C. Han, Z. Hu, S. Nie and J. M. Jornet, "Terahertz Band Communication: An Old Problem Revisited and Research Directions for the Next Decade," *IEEE Transactions on Communications*, **70**, 6, June 2022, pp. 4250-4285.

[2] J. X. Chen, P. G. Zhou, J. Y. Yu, Z. K. Li, H. B. Li and L. Peng, "Research towards terahertz power amplifiers in silicon-based process," *ZTE Communications*, **21**, 2, June 2023, pp. 88-94.

[3] R. Yoshino, Y. Asakura, K. Inagaki and T. Kawanishi, "300GHz terahertz wave scattering experiment and simulation from slightly rough surfaces on dielectrics," *IEICE Communications Express*, December 2023, pp. 1-4.

[4] K. Guan, D. He, B. Ai, Y. Chen, C. Han, B. Peng, Z. Zhong and T. Kürner, "Channel Characterization and Capacity Analysis for THz Communication Enabled Smart Rail Mobility," *IEEE Transactions on Vehicular Technology*, **70**, 5, May 2021, pp. 4065-4080.

[5] D. Dupleich, R. Müller, S. Skoblikov, M. Landmann, G. D. Galdo, and R. Thomä, "Characterization of the Propagation Channel in Conference Room Scenario at 190 GHz," *2020 14th European Conference on Antennas and Propagation (EuCAP)*,2020, pp. 1-5.

[6] W. Tian, B. Wei and M. -H. Gong, "Analysis of Far-Field Scattering and Near-Field Coupling of a Target above Rough Surface Using DD-FDTD," *2020 IEEE MTT-S International Conference on Numerical Electromagnetic and Multiphysics Modeling and Optimization (NEMO)*,2020, pp. 1-3, doi: 10.1109/NEMO49486.2020.9343481.

[7] Z. Zhang, D. He, K. Guan, B. Chen, J. Dou, W. E.I. Sha and Z. Zhong, "A Deep Learning Based Surface Current Generation Method for Scattering Modeling at Terahertz Band," *2024 18th European Conference on Antennas and Propagation (EuCAP 2024)*, March 2024, submitted.

[8] L. Wei, C. Huang, G. C. Alexandropoulos, Z. Yang, J. Yang, W. E.I. Sha, Z. Zhang, M. Debbah and C. Yuen, "Tri-Polarized Holographic MIMO Surfaces for Near-Field Communications: Channel Modeling and Precoding Design," *IEEE Transactions on Wireless Communications*, **22**, 12, December 2023, pp. 8828-8842.

[9] B. Schaefer, E. Collett, R. Smyth, D. Barrett, and B. Frahe, "Measuring the Stokes polarization parameters," *Amer. J. Phys*, **75**, 2, February 2007, pp. 163-168.

[10] I. Naito, "A Note on Representation of Electromagnetic Plane Wave Polarization State," *IEEE Transactions on Antennas and Propagation*, **70**, 7, July 2022, pp. 6066-6071.